J|A|C|S
ARTICLES
Published on Web 10/23/2004

Perfect Orientation Ordered in-Situ One-Dimensional Self-Assembly of Mn-Doped PbSe Nanocrystals

Weigang Lu,[†] Puxian Gao,[‡] Wen Bin Jian,[§] Zhong Lin Wang,[‡] and Jiye Fang*,[†]

Contribution from the Department of Chemistry and Advanced Materials Research Institute, University of New Orleans, New Orleans, Louisiana 70148, School of Materials Science and Engineering, Georgia Institute of Technology, Atlanta, Georgia 30332-0245, and Department of Physics, National Chung Hsing University, 250 Kuo Kwang Road, Taichung 40254, Taiwan, Republic of China

Received June 1, 2004; E-mail: jfang1@uno.edu

Abstract: We demonstrate a novel approach for the large-scale, shape-controlled synthesis of one-dimensional (1D) corrugated nanoarrays of $Pb_{(1-x)}Mn_xSe$ nanocrystals ($0.002 \leq x \leq 0.008$) through an *in-situ* self-assembly without using either capping polymer or ionic surfactant. The one-step-prepared 1D nanoarrays exhibit a well-defined morphology, single-crystal orientation, and clean surface without amorphous contamination. The average diameter of the 1D nanoarrays can be controlled and varied from <10 to 80 nm by finely tuning the assembly temperature and the growth time. Four growth models were suggested to explain the *in-situ* self-assembly processes based on the fundamental building blocks of octahedral nanocrystals by sharing {111} facets.

The synthesis of low-dimensional functional materials[1−3] with control of shape and size[4] is a most challenging preparation due to the increasing theoretical interest and technological demand.[5−8] To achieve 1D materials[9,10] in diameters of quantum-confined limit,[11] colloidal self-assembly is a very promising technique in modern materials chemistry[12,13] and nanotechnology.[14] This strategy traditionally consists of preparing monodispersed nanocrystals (NCs)[15,16] (including the synthesis and possible size-refinement), surface passivation, and pattern-organization[17,18] (including self-organization of NCs at room temperature and possible postannealing process). The self-organization of NCs involves various forces such as hydrogen bonding, dipolar forces, van der Waals forces, hydrophilic or hydrophobic interactions, chemsorption, surface tension, and gravity[19] in colloids. NCs can be, at room temperature, stable with respect to aggregation only if capping ligands provide a repulsive force of sufficient strength and range to counteract the inherent van der Waals attraction between NCs. Based on this mechanism, NCs suspended in a pair of solvent/nonsolvent (e.g., the octane/octanol system) can be precipitated by a controlled-evaporation of the solvent from the mixture and eventually self-organized into close-packed and locally ordered 2D[20,21] or 1D[22] patterns. We have realized that, at high temperature, the attractive forces between the NCs may be dominated by a driving force in a certain direction corresponding to a specific nanocrystalline plane due to its relative low surface energy. We therefore propose a methodology of *in-situ* self-assembly of NCs at high temperature to directly produce 1D nanomaterials using a simple solution approach, and we recently achieved a one-step preparation of $Pb_{1-x}Mn_xSe$ 1D corrugated nanoarrays ($0.002 \leq x \leq 0.008$). In this Article, we demonstrate the processing of structurally controlled single-crystal corrugated nanoarrays of Mn-doped PbSe by focusing on the $Pb_{0.996}Mn_{0.004}$-Se system using *in-situ* self-assembly of perfect orientation ordered NCs in the absence of both polymer and ionic surfactant, and we discuss four growth models based on the fundamental building blocks of octahedral nanocrystals by sharing {111} facets as well.

To prepare the 1D $Pb_{(1-x)}Mn_xSe$ corrugated nanoarrays, we employed a combination of both precipitation and decomposition

[†] University of New Orleans.
[‡] Georgia Institute of Technology.
[§] National Chung Hsing University.

(1) Manna, L.; Milliron, D. J.; Meise, A.; Scher, E. C.; Alivisatos, A. P. *Nat. Mater.* **2003**, *2*, 382.
(2) Manna, L.; Scher, E. C.; Alivisatos, A. P. *J. Cluster Sci.* **2002**, *13*, 521.
(3) Scher, E. C.; L. M. a. A. P. A. *Philos. Trans. R. Soc. London, Ser. A* **2003**, *361*, 241.
(4) Lee, S.-M.; Jun, Y.-w.; Cho, S.-N.; Cheon, J. *J. Am. Chem. Soc.* **2002**, *124*, 11244.
(5) Buhro, W. E.; Colvin, V. L. *Nat. Mater.* **2003**, *2*, 138.
(6) Yu, H.; Li, J.; Loomis, R. A.; Wang, L.-W.; Buhro, W. E. *Nat. Mater.* **2003**, *2*, 517.
(7) Kan, S.; Mokari, T.; Rothenberg, E.; Banin, U. *Nat. Mater.* **2003**, *2*, 155.
(8) Duan, X.; Huang, Y.; Cui, Y.; Wang, J.; Lieber, C. M. *Nature* **2001**, *409*, 66.
(9) Penn, R. L.; Banfield, J. F. *Geochim. Cosmochim. Acta* **1999**, *63*, 1549.
(10) Jun, Y.-w.; Jung, Y.-y.; Cheon, J. *J. Am. Chem. Soc.* **2002**, *124*, 615.
(11) Alivisatos, A. P. *J. Phys. Chem.* **1996**, *100*, 13226.
(12) Xia, Y.; Yang, P.; Sun, Y.; Wu, Y.; Mayers, B.; Gates, B.; Yin, Y.; Kim, F.; Yan, H. *Adv. Mater.* **2003**, *15*, 353.
(13) Tang, Z.; Kotov, N. A.; Giersig, M. *Science* **2002**, *297*, 237.
(14) Hu, J.; Odom, T. W.; Lieber, C. M. *Acc. Chem. Res.* **1999**, *32*, 435.
(15) Murray, C. B.; Kagan, C. R.; Bawendi, M. G. *Annu. Rev. Mater. Sci.* **2000**, *30*, 545.
(16) Lisiecki, I.; Albouy, P.-A.; Pileni, M.-P. *Adv. Mater.* **2003**, *15*, 712.
(17) Sun, S.; Murray, C. B.; Weller, D.; Folks, L.; Moser, A. *Science* **2000**, *287*, 1989.
(18) Murray, C. B.; Sun, S.; Doyle, H.; Betley, T. *MRS Bull.* **2001**, *26*, 985.
(19) Tolles, W. M. *MRS Bull.* **2000**, *25*, 36.
(20) Farrell, D.; Majetich, S. A.; Wilcoxon, J. P. *J. Phys. Chem. B* **2003**, *107*, 11022.
(21) Zeng, H.; Li, J.; Liu, J. P.; Wang, Z. L.; Sun, S. *Nature* **2002**, *420*, 395.
(22) Tripp, S. L.; Pusztay, S. V.; Ribbe, A. E.; Wei, A. *J. Am. Chem. Soc.* **2002**, *124*, 7914.

10.1021/ja046769j CCC: $27.50

in phenyl ether in the presence of oleic acid and trioctylphosphine (TOP) as capping agents to stabilize the as-formed colloids. The precipitation occurs between lead acetate and trioctylphosphine selenium (TOPSe) as reported by Wehrenberg et al.[23] The thermal decomposition is based on $Mn_2(\mu\text{-SeMe})_2(CO)_8$,[24−26] which is in a minor amount in the system and was presynthesized from methyllithium, selenium, and $Mn(CO)_5Br$ by adapting an established procedure.[24,27] Based on Mikulec's report[24] and our experience,[25] at high temperature the use of the organometallic compound $Mn_2(\mu\text{-SeMe})_2(CO)_8$ can minimize the problem of Mn segregation onto the particle surface as the pre-existing Se−Mn bond may assist in "dragging" the Mn^{2+} into the PbSe lattice. According to the general catalytic growth mechanism of nanowires proposed by Lieber et al.[14] and the La Mer model,[28] many systems exhibit an Ostwald ripening process, in which the high surface energy of the small NCs promotes their dissolution, and the material is grown into the larger NCs.[29,30] To provide enough primary clusters for keeping a constant rate of the crystal growth, we employed a dynamic injection technique[31] when simultaneously monitoring the progress of the reaction. In a typical experiment, $Pb(ac)_2 \cdot 3H_2O$ (2.85 mmol), phenyl ether (15 mL), and oleic acid (3.0 mL) were mixed and heated to 150 °C for 30 min under an argon stream in a three-neck flask equipped with a condenser. After the solution was cooled to 40 °C, it was subsequently mixed with 2.4 mL of $Mn_2(\mu\text{-SeMe})_2(CO)_8$ precursor (0.05 M) which was predissolved in trioctylphosphine (TOP, Aldrich, 90%) and 4.0 mL of TOP−Se solution (1 M for Se) in a glovebox to form a stock solution. After the first portion of such a stock solution (10 mL) was rapidly injected into 15 mL of phenyl ether that was preheated to a certain temperature (from 180 to 250 °C) for 5 min with agitation, a portion of the hot reaction mixture (3.0 mL) was extracted from the flask, and equal volume of the premixed stock solution of reagents was injected into the flask under argon stream. These operations of dynamic injections were successively conducted in an interval of every 5 min at a constant temperature. Each product was retrieved from the original solvent by centrifugation with an equal volume of ethanol as a polar solvent, redispersed in toluene, and monitored by TEM observation for checking the respective *in-situ* self-assembly progress. To ensure the accuracy of the Mn composition determination, a surface ligand exchange posttreatment was subsequently performed on all of the as-separated products by following Kuno's procedure.[32] Particularly, the corrugated nanoarrays were immersed into pyridine for 3 days with solvent-refreshing at least three times. After the pyridine washing, all of the Mn ions that may physically adsorb on the surface of products should be removed. The elemental composition in all of the products of $Pb_{1-x}Mn_xSe$ ($0.002 \leq x \leq 0.008$) was analyzed using an inductively coupled plasma (ICP) technique after a pyridine ligand-exchange. As will be depicted later, the concentration of Mn^{2+} from ligand-exchanged corrugated nanoarrays has also been estimated on the basis of magnetic data. To avoid possible confusion of Mn^{2+} concentration from several determinations, we define the formula $Pb_{1-x}Mn_xSe$ on the basis of ICP results.

It is well known that for a certain size of NCs, there exists a temperature limit that can trigger atom diffusion and crystal growth.[31,33] To ensure the occurrence of the *in-situ* self-assembly, the solution temperature and the growth time as two of the key conditions have been optimized. We first focused our study on a Mn-fixed component, $Pb_{0.996}Mn_{0.004}Se$, and the investigation of $Pb_{0.996}Mn_{0.004}Se$ (PbMnSe) corrugated nanoarrays formation indicates that the *in-situ* self-assembly of PbMnSe commences at 180 °C, and well-developed PbMnSe corrugated nanoarrays can be observed from the sample grown at 250 °C (see Figure S1 in the Supporting Information). The yield of PbMnSe corrugated nanoarrays based on the inorganic input is higher than 94% when the self-assembly is conducted at 250 °C, and the reproducibility is ∼100% from run to run under the specified conditions. As demonstrated in the Supporting Information (Figure S2), furthermore, an increase of evolution time favors a morphology conversion from single rows of stacked NC arrays up to multilines of octahedral corrugated nanoarrays.[34] To further understand the evolution mechanism of these orientation-ordered crystal arrays during this *in-situ* synthetic process, we have carefully examined all of the samples taken from these PbMnSe corrugated nanoarrays self-assembled at 250 °C with different growth times (typically from 5 to 20 min), by scanning electron microscopy (SEM) and transmission electron microscopy (TEM) using a field-emission scanning electron microscope (LEO 1530 FE-SEM, operated at 5 and 10 keV) and a field-emission transmission electron microscope (Hitachi 2000 FE-TEM, operated at 200 keV), respectively, unless otherwise specified. Figure 1 shows typical morphologies and structural characteristics of PbMnSe corrugated nanoarrays after a short period of growth time (5 min). Two SEM images (Figure 1a and b) demonstrate typical morphologies of the as-prepared PbMnSe corrugated nanoarrays. The PbMnSe corrugated nanoarrays were apparently self-assembled by uniform-sized PbMnSe NCs according to specific stacking modes, displaying an array of stacked NCs with side-facets which expose periodical zigzag corrugated side-surfaces. Figure 1c−f shows typical TEM images of PbMnSe corrugated nanoarrays. The stacking forms a one-particle array structure. The most striking feature is that electron diffraction recorded from an array composed of over 20 NCs shows a single-crystal structure (Figure 1d), with the array axis [001], suggesting the precise orientation alignment among all of the NCs. Furthermore, we have never observed a defect on the structure of these nanoarrays. The faceted shape of the NCs is apparent and can be directly indexed to be the {111} facets (Figure 1e and f). High-resolution TEM reveals the faceted shape of the NC and the well-defined crystallographic planes, as well as its single-crystal, dislocation-free volume (Figure 1g). The surface of the NC is also clean without amorphous contamination.

Figure 2 is typical SEM and TEM images of the PbMnSe corrugated nanoarrays assembled using a long period of growth

(23) Wehrenberg, B. L.; Wang, C.; Guyot-Sionnest, P. *J. Phys. Chem. B* **2002**, *106*, 10634.
(24) Mikulec, F. V.; Kuno, M.; Bennati, M.; Hall, D. A.; Griffin, R. G.; Bawendi, M. G. *J. Am. Chem. Soc.* **2000**, *122*, 2532.
(25) Ji, T.; Jian, W.-B.; Fang, J. *J. Am. Chem. Soc.* **2003**, *125*, 8448.
(26) Jian, W.-B.; Fang, J.; Ji, T.; He, J. *Appl. Phys. Lett.* **2003**, *83*, 3377.
(27) Coleman, A. P.; Dickson, R. S.; Deacon, G. B.; Fallon, G. D.; Ke, M.; McGregor, K.; West, B. O. *Polyhedron* **1994**, *13*, 1277.
(28) LaMer, V. K.; Dinegar, R. H. *J. Am. Chem. Soc.* **1950**, *72*, 4847.
(29) Smet, Y. D.; Deriemaeker, L.; Finsy, R. *Langmuir* **1997**, *13*, 6884.
(30) Grätz, H. *Scr. Mater.* **1997**, *37*, 9.
(31) Qian, C.; Kim, F.; Ma, L.; Tsui, F.; Yang, P.; Liu, J. *J. Am. Chem. Soc.* **2004**, *126*, 1195.
(32) Kuno, M.; Lee, J. K.; Dabbousi, B. O.; Mikulec, F. V.; Bawendi, M. G. *J. Chem. Phys.* **1997**, *106*, 9869.
(33) Puntes, V. F.; Krishnan, K. M.; Alivisatos, A. P. *Science* **2001**, *291*, 2115.
(34) Wang, Z. L. *J. Phys. Chem. B* **2000**, *104*, 1153.

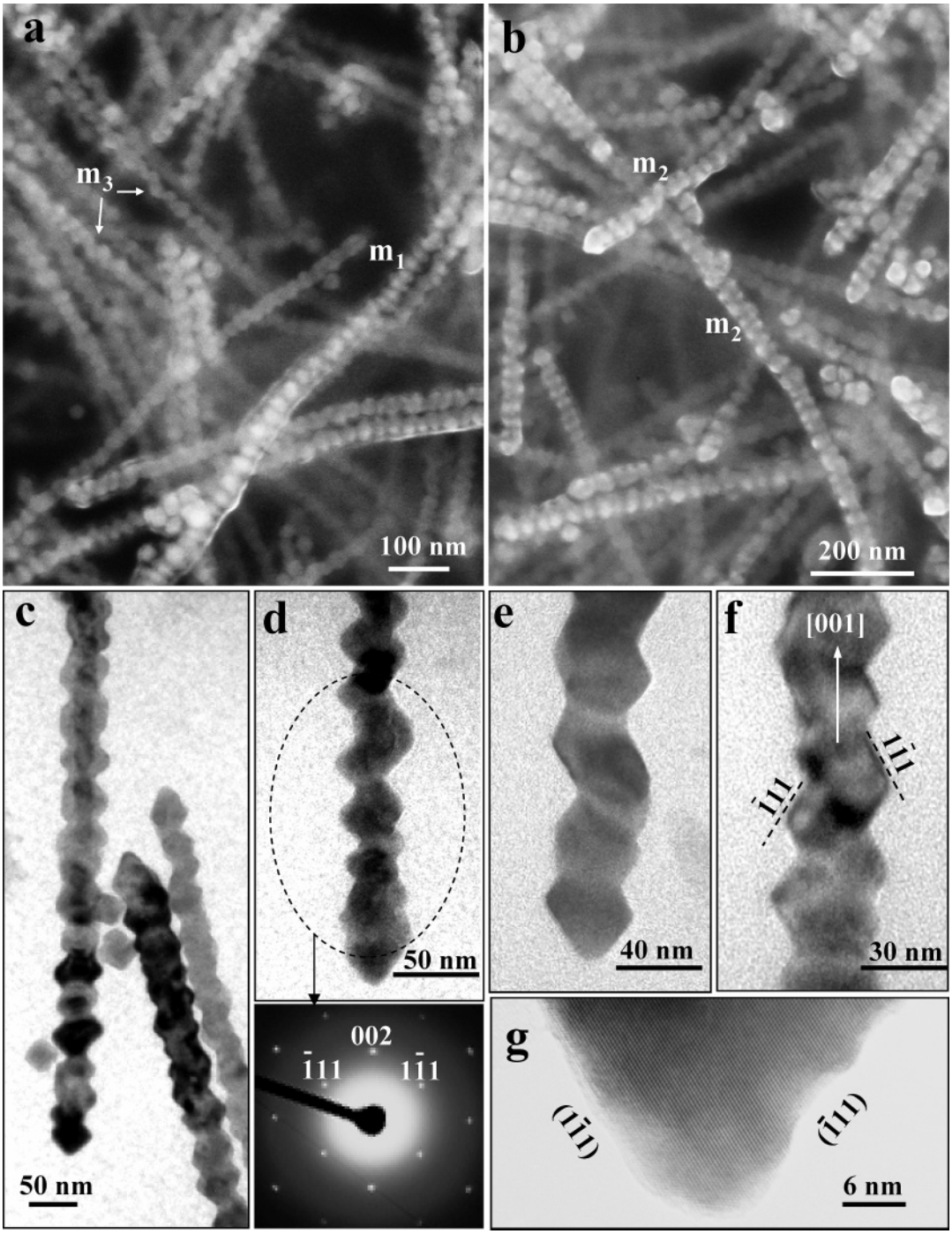

Figure 1. Morphologies and structural characteristics of $Pb_{0.996}Mn_{0.004}Se$ corrugated nanoarrays after 5 min of growth. (a and b) SEM micrographs, indicating that these corrugated nanoarrays were self-assembled by uniform-sized NCs according to specific stacking modes. (c, e, and f) TEM images, displaying arrays of stacked NCs with side-facets which expose periodical zigzag corrugated side-surfaces. (d) TEM micrograph and electron diffraction pattern, showing a single-crystal structure based on an array composed of over 20 NCs. (g) HRTEM image, revealing the faceted shape of the NC and the well-defined crystallographic planes and demonstrating that the surface of the NC is clean without amorphous contamination.

time (20 min). The corrugated nanoarrays have a uniform morphology and uniform size of ~80 nm in diameter, 1−2 μm in length (Figure 2a). Each corrugated nanoarray is obviously composed of four lines of square-based NC arrays, and the fifth row is at the center (Figure 2b and c). The TEM bright field image (Figure 2d) gives a [110] projected profile, where the dark-contrasted paired areas along the growth direction [001] (as shown in Figure 2e) are due to the large thickness of the overlapped cores from two rows of assembling NCs in the projection direction. The TEM image and the corresponding electron diffraction pattern (Figure 2d and e) show the perfect orientation alignment among all of the NCs and the single-crystal structure of the entire array. The array axis is [001], and the normals of the four side-surfaces are ⟨110⟩.

The structures of the corrugated nanoarrays have three characteristics: each array is a single crystal and is composed of orientation precisely aligned NCs; the surfaces of the NC are dominated by {111} facets; and the axis direction of the

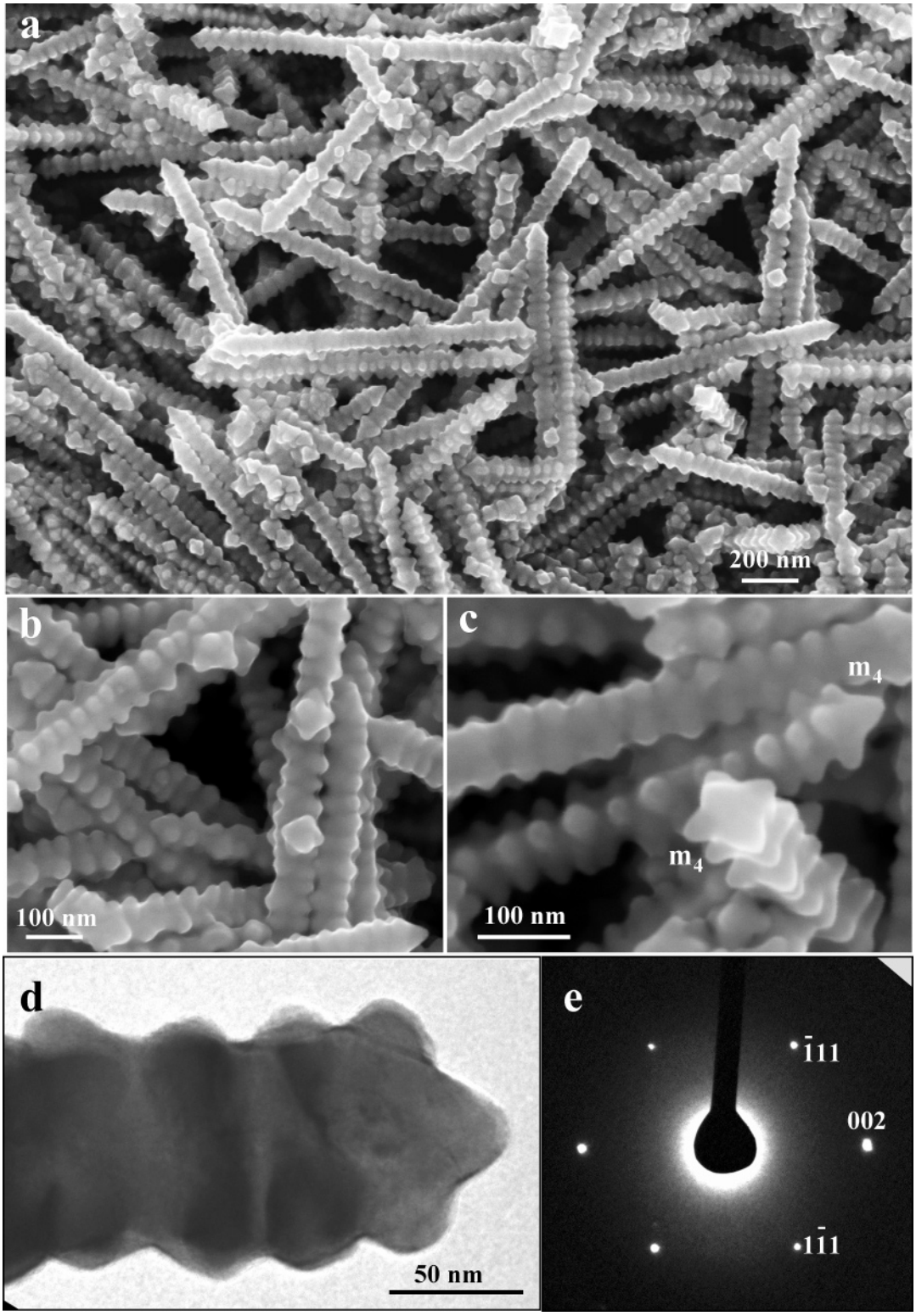

Figure 2. Morphologies and structural characteristics of $Pb_{0.996}Mn_{0.004}Se$ corrugated nanoarrays after 20 min of growth. (a−c) SEM micrographs, showing the corrugated nanoarrays have a uniform morphology composed of four lines of square-based NC arrays and a fifth row of NCs in the center and a uniform size of ∼80 nm in diameter, 1−2 μm in length. (d) HRTEM image, giving a [110] projected profile and displaying the single-crystal structure of the entire array. (e) The electron diffraction pattern recorded from the area selected in (d), showing the perfect orientation alignment among all of the NCs.

array is [001], and the side-surfaces are {110}. From the information provided by Figure 1c−g and the images of dispersive NCs, the shape of the NC is dominated by octahedron and truncated octahedron (Figure 3a), the surfaces of which are {111} and {100}, and the side-edges of the octahedron are ⟨110⟩. The principles for assembling the NCs are to face the same type of faces, such as {111} to {111}, and align them in the same orientation to enhance the packing density,[35,36] resulting in a single-crystal structure of the entire array. This is driven by minimizing the interface mismatch energy by forming a coherent

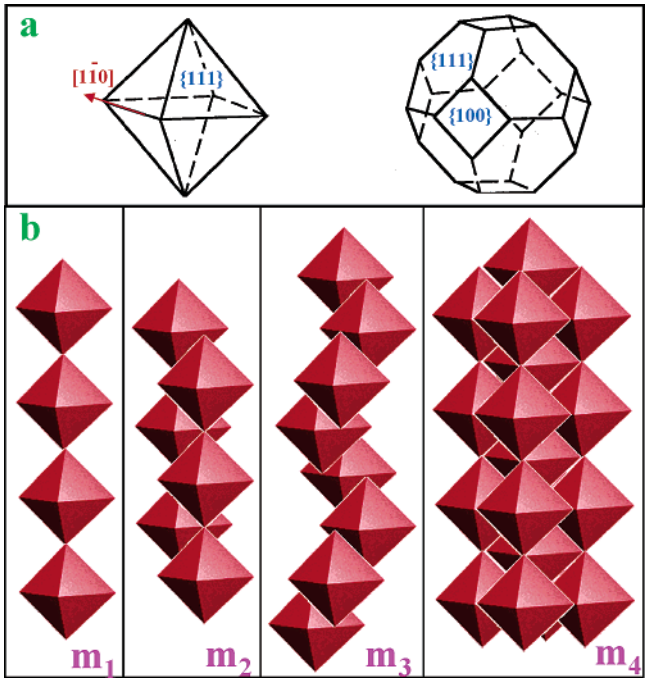

Figure 3. Structure models of $Pb_{0.996}Mn_{0.004}Se$ corrugated nanoarrays. (a) Drawings of octahedron (left) and truncated octahedron (right). (b) Proposed growth models, m1, m2, m3, and m4, for forming linear PbMnSe corrugated nanoarrays. The model m4 could only be transformed from either of the m1, m2, and m3 models by introducing a transverse displacement of the NCs.

interface and reducing the exposed surface area. The sharing of the ⟨110⟩ edges is to minimize the dangling bonds on the {110} type facets due to their higher energy for the cubic system.

There are four basic orientation ordered stacking models for assembling PbMnSe NCs into array structures, as represented by models m_1, m_2, m_3, and m_4 in Figure 3b. By joining the two octahedral into an array, one of the favorable configurations is partially sharing a (111) plane, forming a linear chain (model m_1 in Figure 3b). This is the configuration revealed by the TEM images presented in Figure 1d−f recorded from the samples with short growth time. The alignment of two m_1 chains forms the model m_2, which can be identified in Figure 1b. The m_3 assembly is to form a twist helical while assembling the NCs around its four equivalent {111} facets, which have been identified in Figure 1a. As the growth proceeds, several linear chains can join together to form an m_4 assembly model, which is composed of four square-based NC chains, and the fifth one is at the middle to reduce the void volume. The m_4 model is the dominant component in the sample grown for 20 min (Figure 2). The shape of the particles in Figure 2 appears to be spherical-like due to the truncation of the NC by forming the {100} facets (see Figure 3a).

Models m_1, m_2, and m_3 are formed by partially sharing the {111} facets, while m_4 is formed by sharing the ⟨110⟩ edges. All of the NCs are perfectly aligned, and the entire array is a single crystal. After a long period time of growth (20 min) at 250 °C, the self-assembled PbMnSe corrugated nanoarrays tend to grow much larger than those after a short time period of growth. The stacking mode of NCs then has to choose a more efficient way to minimize both the surface energy and the interface mismatch strain. The longer time period of growth tends to form NCs dominated by truncated octahedrons; thus the stacking tends to share their {002} planes and ⟨110⟩ intersection edges rather than the {111} planes, because the former two have higher energy than that of {111}.

It is reasonable to believe that there is a short time period of growth at 250 °C at which the modes of self-assembly could be a mixture of the m_1, m_2, and m_3 models. With an increase of growth time, the m_4 model tends to be the dominant self-assembly mode of the larger sized PbMnSe corrugated nanoarrays. An increase in growth time increases only the transverse size of the nanoarrays, but not their lengths. The different sizes of NC presented in Figures 1 and 2 suggest that the NC building blocks grow independently as free-standing particles in the solution before the assembly, and no more growth is possible after forming the single-crystal assembled arrays. This suggests that the growth of the particles is a fast process at 250 °C, while self-assembly occurs only at the last stage. The structure models m_1, m_2, and m_3 can be promoted only if the concentration of the free-standing particles in the solution is constantly supplied, as provided by the dynamic injections, whereas model m_4 could only be transformed from either of m_1, m_2, and m_3 models by introducing a transverse displacement of the NCs, which is unlikely to occur after forming a coherent interface bonding. Therefore, the self-assembly presented in Figures 1 and 2 might occur at different moments of the growth.

The present *in-situ* self-assembly strategy has actually extended the concept of nanocrystalline "self-assembly" from conventional room-temperature to high-temperature region, by providing a simple and fast procedure for a large-scale, high-yield preparation of 1D $Pb_{1-x}Mn_xSe$ corrugated nanoarrays at relatively low reaction temperature with a high orientation order of single crystals, clean surfaces, diameter control, and high preparation repeatability. This approach of 1D fabrication skips both the traditional solid template and the ionic surfactant, as well as avoids the violently high evaporation temperature that is generally used in the vapor−liquid−solid method. As a diluted magnetic semiconductor, 1D Mn-doped PbSe with a quantum-confined diameter has attracted an increasing interest in exploring the spin−spin interactions[37,38] due to the technological demand of building spintronic devices. We also demonstrated that the diamagnetic term increases as the diameter of these corrugated nanoarrays decreases, which is consistent with the unique phenomenon in quantum dot systems that we recently observed. In addition, the four crystal evolution models presented here can also be applied to the explanation of the 1D-nanoarray-formation mechanism for other similar systems with building blocks of octahedral NCs. It is therefore believed that this *in-situ* one-dimensional self-assembly approach in the solution phase will be able to realistically extend to the 1D-nanoarray-formation of other structure-similar systems such as cubic PbTe[39] and $AgPb_mSbTe_{2+m}$,[40] which are very important

(35) Harfenist, S. A.; Wang, Z. L.; Alvarez, M. M.; Vezmar, I.; Whetten, R. L. *Adv. Mater.* **1997**, *9*, 817.
(36) Wang, Z. L. *Adv. Mater.* **1998**, *10*, 13.
(37) Geist, F.; Pascher, H.; Kriechbaum, M.; Frank, N.; Bauer, G. *Phys. Rev. B* **1996**, *54*, 4820.
(38) Wolf, S. A.; Awschalom, D. D.; Buhrman, R. A.; Daughton, J. M.; Molnar, S. v.; M. L. Roukes, A. Y. C.; Treger, D. M. *Science* **2001**, *294*, 1488.
(39) Harman, T. C.; Taylor, P. J.; Walsh, M. P.; LaForge, B. E. *Science* **2002**, *297*, 2229.
(40) Hsu, K. F.; Loo, S.; Guo, F.; Chen, W.; Dyck, J. S.; Uher, C.; Hogan, T.; Polychroniadis, E. K.; Kanatzidis, M. G. *Science* **2004**, *303*, 818−821.

thermoelectric materials when their dimensions are minimized to the quantum confinement limit.[41,42]

Acknowledgment. We acknowledge the Defense Advanced Research Projects Agency (DARPA) through the Office of Naval Research (N00014-02-1-0729), the NSF/LA Board of Regents [(2001-04)-RII-03], and the NSF NIRT (ECS-0210332) for support.

Supporting Information Available: TEM and SEM images. This material is available free of charge via the Internet at http://pubs.acs.org.

JA046769J

(41) Hicks, L. D.; Dresselhaus, M. S. *Phys. Rev. B* **1993**, *47*, 16631.
(42) Hicks, L. D.; Dresselhaus, M. S. *Phys. Rev. B* **1993**, *47*, 12727.